Journal of Science and Technology in Civil Engineering, HUCE, 2025, 19 (2): 78–91

EXTREME GRADIENT BOOSTING MODEL FOR FORECASTING SLUMP AND COMPRESSIVE STRENGTH OF HIGH-PERFORMANCE CONCRETE

Van Tuan Vu[a,*], Quang Trung Dinh[a]

[a]*Institute of Construction Technology, Le Quy Don Technical University, 236 Hoang Quoc Viet road, Cau Giay district, Hanoi, Vietnam*

Article history:
Received 13/5/2024, Revised 22/3/2025, Accepted 29/5/2025

Abstract

The Extreme Gradient Boosting (XGBoost) model has found success across a wide range of engineering challenges because it is straightforward, flexible, and applicable to both classification and regression tasks. Concrete, a composite material made up of several intricate components, is affected by various factors, making it difficult to predict its properties with precision. This article presents an Extreme Gradient Boosting (XGBoost) model designed to predict the slump and strength of high-performance concrete (HPC) incorporating a combination of blast furnace slag and silica fume as mineral admixtures. The model was developed using an experimental dataset following the Box-Hunter statistical method. The criteria used to assess the models' accuracy are R squared (R^2) and mean squared error (MSE). The findings indicate that the XGBoost model, developed using an experimental dataset following the Box-Hunter statistical method, is well-suited for predicting both the slump and compressive strength of concrete.

Keywords: extreme gradient boosting (XGBoost); the slump of concrete; prediction; the strength of concrete.

https://doi.org/10.31814/stce.huce2025-19(2)-06

1. Introduction

Concrete is a widely used building material across the globe [1–3], with several distinct types having been developed over the years [4–13]. High-performance concrete (HPC) has gained traction for its excellent mechanical strength and durability. This popularity can be attributed to innovations like advanced superplasticizers and the inclusion of mineral additives, which create denser microstructures and reduce permeability. This latest generation of HPC offers enhanced workability, a compressive strength exceeding 60 MPa, and improved resistance to physicochemical degradation. These characteristics allow HPC to withstand significant stress and remain durable even in severe environmental conditions.

Concrete's inherent complexity, stemming from its many components, complicates the task of predicting its properties. Building models to estimate concrete properties based on various influencing factors is difficult because of the material's low predictability. This challenge is compounded when designing experiments, where researchers must manage a large array of variables that impact the results. To account for these numerous factors, more experimental trials are required, increasing the workload and complicating the process of accurately estimating the true response function. Moreover, the presence of uncontrolled variables further complicates the task of achieving reliable predictions.

Lately, the construction industry has increasingly embraced machine learning techniques (MLT) to boost project efficiency, better manage resources, and improve the ability to predict outcomes in

*Corresponding author. *E-mail address:* vantuanvu@lqdtu.edu.vn (Vu, V. T.)

construction workflows and material properties [14–16]. Additionally, machine learning techniques have been used more frequently to increase the precision of predictions regarding concrete properties.

Li and Liew [17] developed a prediction model using the XGBoost algorithm to forecast the factors influencing the compressive strength of steel fiber reinforced concrete and mortar when subjected to high temperatures. Their model outperformed seven other machine learning methods assessed in their study, which included AdaBoost, Random Forests, k-Nearest Neighbors Regression, Artificial Neural Network, Support Vector Regression, Multivariate Adaptive Regression Splines, and Linear Regression. Similarly, Duan, Asteris [18] conducted research on the 28-day compressive strength of recycled aggregate concrete, employing four different artificial intelligence techniques. They developed a model using a combination of a meta-heuristic search sociopolitical algorithm (ICA) and XGBoost, termed the ICA-XGBoost model. This model was the top performer among those created, yielding the best results according to performance metrics. In a different study, Tipu, Panchal [19] pursued three key objectives: maximizing compressive strength, reducing costs, and lowering CO_2 emissions. They modeled the compressive strength of concrete using the XGBoost Regressor, while costs and CO_2 emissions were calculated using mathematical models. The results supported the reliability and effectiveness of the XGBoost model for predicting compressive strength. Furthermore, Le, Vu [20] presented a new predictive tool built on a machine learning framework to estimate the compressive strength and effective porosity of previous concrete based on its composition. Their findings indicated that the extreme gradient boosting (XGB) method offered significantly greater accuracy than other techniques.

There are not many studies investigating the application of the XGBoost model to forecast both the slump and compressive strength of high-performance concrete. This study examined the suitability of the XGBoost model for simultaneously predicting these two properties in high-performance concrete samples. The dataset used to construct these models included various concrete samples, each with different ratios of water/adhesive, blast furnace slag/adhesive, silica fume/adhesive, and super-plastic additive/adhesive. The samples were prepared following the Box Hunter statistical method [21], to find the optimal composition for high-performance concrete. The models' accuracy in predicting the desired outcomes was evaluated using RSQ and MSE metrics to identify the most effective prediction model.

2. Experimental study process and data

A considerable body of research has demonstrated that adding silica fume, along with other mineral additives such as pozzolan, granulated slag, blast furnace slag, or fly ash, to cement significantly enhances the durability and mechanical properties of high-performance concrete (HPC) [22, 23]. Ground granulated blast furnace slag (GGBFS) stands out for its low water absorption due to the smooth surfaces of its grains, which improves the workability of HPC compared to ordinary Portland cement concrete [24, 25].

The inclusion of silica fume and superplasticizer plays a critical role in strengthening the durability and mechanical properties of concrete. This enhancement is attributed to both the filling mechanism and chemical reactions occurring within the concrete. The differing particle sizes between silica fume and cement lead to a denser paste through the physical effects of the filler material, which boosts compaction and increases the accumulation of solid particles.

This experimental study utilized blast furnace slag, silica fume, and a super-plastic additive to create concrete specimens. The goal was to produce concrete with a compressive strength above 60 MPa, a slump exceeding 16 cm, and a cement content of less than 300 kg/m^3.

2.1. Materials

This study utilized PCB40 cement from the NGHI SON cement corporation, located in Hai Thuong Ward, Nghi Son Town, Thanh Hoa Province, Vietnam. This specific cement type meets the mechanical property standards set by the TCVN 6260:2020 [26]. The mechanical characteristics of this cement were evaluated based on the methodologies detailed in TCVN 6016:2011 [27], TCVN 6017:2015 [28], and TCVN 13605:2023 [29]. The results of these assessments are summarized in Table 1.

Table 1. Property of PCB40 cement

Items	Value
Density (g/cm^3)	3.0
Fineness (the amount leftover on a 80 μm sieve) (%)	2.5
Standard ductility (%)	29.5
Coagulate start time (minutes)	90
Coagulate end time (minutes)	135
The intensity of age 28 days (Mpa)	50.4

The coarse-ground powder of GGBFS (ground granulated blast furnace slag) used in this study was sourced as a byproduct from the manufacturing of cast iron at the Thai Nguyen Iron and Steel Joint Stock Corporation in Vietnam. The slag was initially collected in its raw form and then ground down to achieve a particle size smaller than 2.5 mm. Table 2 provides an overview of the physical properties of the GGBFS.

Table 2. Property of GGBFS

Absolute density (g/cm^3)	Blaine Specific Surface (cm^2/g)	Activity index at 7 days (%)
2.94	6300	98

Table 3. Property of silica fume

Absolute density (g/cm^3)	Blaine Specific Surface (cm^2/g)	Activity index at 7 days (%)
2.2	5000	100

This study used a grey, ultra-fine powder of silica fume sourced from the Elkem Company in China. The details of the physical characteristics of the silica fume are presented in Table 3.

The crushed stone used in this study was sourced from Luong Son Town in Hoa Binh Province, Vietnam. The stone had a maximum diameter of 20 mm and complied with the physical and mechanical standards outlined in TCVN 7570:2006 [30]. Table 4 contains the test results for the key physical and mechanical properties of the crushed stone, following the guidelines of TCVN 7572:2006 [31].

Song Lo sand was employed in this study, and it satisfied the physical and mechanical requirements set by TCVN 7570:2006 [30]. The results of tests conducted to determine the key physical and mechanical properties of the sand, as specified in TCVN 7572:2006 [31], are shown in Table 5.

A superplasticizer was used to reduce the water-to-cement ratio in the concrete mixture while ensuring it retained workability. Dynamon SP1, a product of Mapei, was selected for this purpose. This modified acrylic polymer is ideal for precast concrete, offering a lower water-to-cement ratio and excellent mechanical strength in both the initial and final stages of curing. The specific properties of Dynamon SP1 are detailed in Table 6.

Table 4. Property of crushed stone

Items	Value			
Sieve size, (mm)	5	10	10	20
Residual mass accumulated on the sieve, (%)	100	0	100	0
Density, (g/cm^3)	1.57		1.63	
Absorption of water, (%)	2.7		2.8	
Porosity volume mass, (kg/m^3)	2.68		2.78	
Crushed compression strength in cylinders, (%)	0.74		0.63	
Content of rhombus and flatform particles, (%)	0.08		0.07	
Content of dust, mud, clay, (%)	12		10.8	

Table 5. Property of sand

Items	Value					
Sieve size, (mm)	5	2.5	1.25	0.63	0.31	0.14
Residual mass accumulated on the sieve, (%)	0	7.7	17.2	45.1	78.7	96.3
Density, (g/cm^3)	2.66					
Absorption of water, (%)	1.35					
Modulus of magnitude	2.45					
Content of dust, mud, clay, (%)	TCVN 7570:2006					

Table 6. Characteristics of the superplasticizer

Form	Color	Density according to ISO 758 (g/m^3)	Chlorides soluble in water according to EN 480-10 (%)	Alkali content according to EN 480-12 (%)
Liquid	Amber	1.08 ± 0.02 at +20 °C	< 0.1 (absent according to EN 934-2)	< 3.0

Box Hunter's statistical method for experimenters was used to identify the rules governing factor variation. An experimental design with 31 points was established to examine the impact of four factors—namely, the water/adhesive ratio (W/AH, coded as variable x_1), blast furnace slag/adhesive ratio (BFS/AH, coded as variable x_2), silica fume/adhesive ratio (SF/AH, coded as variable x_3), and superplasticizer/adhesive ratio (SPA/AH, coded as variable x_4)—on compressive strength at 28 days (R28) and slump (SN). The experimental results are provided in Table 7.

Table 7. Experimental outcomes based on Box Hunter's methodology

	Coded variables				Factorial experiments				SN	R28
	x_1	x_2	x_3	x_4	W/AH	BFS/AH	SF/AH	SPA/AH	(cm)	(Mpa)
1	-1	-1	-1	-1	0.3	30	3	0.6	9	88.7
2	1	-1	-1	-1	0.34	30	3	0.6	16.5	78.0
3	-1	1	-1	-1	0.3	50	3	0.6	12	85.9
4	1	1	-1	-1	0.34	50	3	0.6	19.5	77.1
5	-1	-1	1	-1	0.3	30	9	0.6	0.5	89.5

	Coded variables				Factorial experiments				SN	R28
	x_1	x_2	x_3	x_4	W/AH	BFS/AH	SF/AH	SPA/AH	(cm)	(Mpa)
6	1	-1	1	-1	0.34	30	9	0.6	4	81.8
7	-1	1	1	-1	0	50	9	0.6	2	85.8
8	1	1	1	-1	0.34	50	9	0.6	7	81.2
9	-1	-1	-1	1	0.3	30	3	1	19	89.0
10	1	-1	-1	1	0.34	30	3	1	21	77.6
11	-1	1	-1	1	0.3	50	3	1	20.5	86.1
12	1	1	-1	1	0.34	50	3	1	22	77.2
13	-1	-1	1	1	0.3	30	9	1	11	89.8
14	1	-1	1	1	0.34	30	9	1	17.5	81.9
15	-1	1	1	1	0.3	50	9	1	17	86.5
16	1	1	1	1	0.34	50	9	1	21	81.5
17	-2	0	0	0	0.28	40	6	0.8	11	94.7
18	2	0	0	0	0.36	40	6	0.8	21	77.4
19	0	-2	0	0	0.32	20	6	0.8	15.5	84.1
20	0	2	0	0	0.32	60	6	0.8	19.5	79.8
21	0	0	-2	0	0.32	40	0	0.8	21	80.1
22	0	0	2	0	0.32	40	12	0.8	4	84.7
23	0	0	0	-2	0.32	40	6	0.4	2.5	82.7
24	0	0	0	2	0.32	40	6	1.2	19.5	82.8
25	0	0	0	0	0.32	40	6	0.8	18	84.7
26	0	0	0	0	0.32	40	6	0.8	17.5	84.1
27	0	0	0	0	0.32	40	6	0.8	18.5	83.2
28	0	0	0	0	0.32	40	6	0.8	17	84.2
29	0	0	0	0	0.32	40	6	0.8	16.5	83.3
30	0	0	0	0	0.32	40	6	0.8	17.5	84.2
31	0	0	0	0	0.32	40	6	0.8	18.5	82.1
Min	-2	-2	-2	-2	0.28	20	0	0.4	0.5	77.1
Max	2	2	2	2	0.36	60	12	1.2	22	94.7

Table 8. Test specimens

No	Coded variables				Factorial experiments				SN	R28
	x_1	x_2	x_3	x_4	W/AH	BFS/AH	SF/AH	SPA/AH	(cm)	(Mpa)
1	-2	1.675	-0.765	1	0.28	56.75	3.705	1	18.5	92.2
2	-1	0.551	-1.121	0	0.3	45.51	2.637	0.8	17.5	88.5
3	0	1.409	-1.548	-1	0.32	54.09	1.356	0.6	18.5	75.4
4	1	0.678	-0.863	-1	0.34	46.78	3.411	0.6	18.5	72.6
5	2	1.034	-0.39	-1	0.36	50.34	4.83	0.6	18	70.3
Min	-2	0.551	-1.548	-1	0.28	45.51	1.356	0.6	17.5	70.3
Max	2	1.675	-0.39	1	0.36	56.75	4.83	1	18.5	92.2

Using Box Hunter's statistical method [21], a regression function was developed to identify the optimal composition. Five samples were created for additional testing, and the results are displayed

in Table 8. Based on these results, it is possible to produce concrete with a compressive strength exceeding 60 MPa, a slump greater than 16 cm, and a cement content below 300 kg/m^3.

Figure 1. Preparation of concrete samples and compressive strength testing

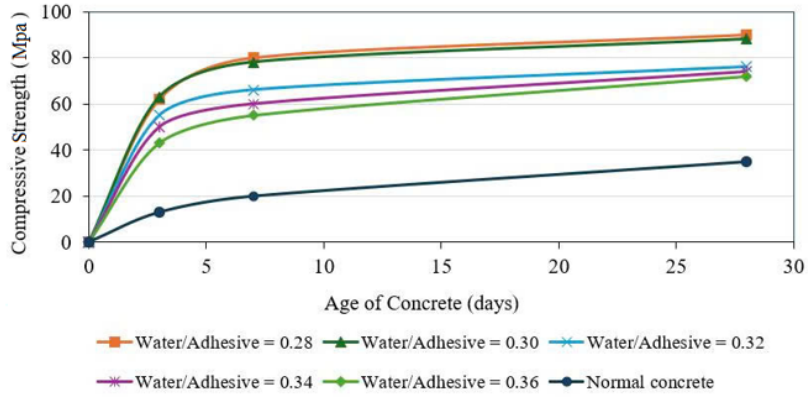

Figure 2. Variations in compressive strength of concrete across different periods

Fig. 2 illustrates the variations in compressive strength of concrete across different periods. The results indicate that a mixture containing 45%-55% GGBFS, adhesive, and silica fume did not slow down the initial strength development of the concrete when compared to traditional concrete.

2.2. *Data division and preprocessing*

The training dataset contained 31 samples, as detailed in Table 7, while the testing dataset included 5 samples, as outlined in Table 8. The test data is entirely new compared to the training data and is planned according to Box-Hunter's methodology, with some values falling beyond the range of the training data. To ensure balanced treatment of all variables during training and to minimize dimensionality, preprocessing involved scaling both input and output variables to a range between 0 and 1. The scaling formula used to adjust the value of each variable, x, is shown below:

$$x_i = \frac{(x - x_{\min})}{(x_{\max} - x_{\min})} \tag{1}$$

where $x_{\max}$ and $x_{\min}$ refer to the maximum and minimum values of each variable x, respectively.

3. XGBoost model

3.1. Overview of XGBoost model

The XGBoost model, short for Extreme Gradient Boosting, is an improved variant of the gradient boosting technique originally introduced by [32]. This sophisticated tree-boosting system uses a set of additive functions to make predictions, which can be mathematically expressed as:

$$y_i = y_0 + \eta \cdot \sum_{k=1}^{M} f_k(X_i) \tag{2}$$

In this equation, y_i denotes the predicted output for the ith sample, with X_i being the vector of features for that sample. M represents the total number of estimators, while each estimator f_k (where k ranges from 1 to M) is an individual tree structure. The initial prediction y_i^0 is the average value of the observed outputs in the training dataset. The parameter η is the learning rate, sometimes called the shrinkage parameter, which helps optimize model performance by allowing gradual adjustments as new trees are added, thereby reducing the risk of overfitting.

The training procedure follows an additive approach, as described in Eq. (2). At each k_{th} step, a new estimator is added to the model. The prediction for this step, y_i^k, is calculated by combining the prediction from the previous step, y_i^{k-1}, with the estimate from the newly added k_{th} estimator, f_k, as illustrated in the following expression:

$$y_i^k = y_i^{k-1} + \eta \cdot f_k \tag{3}$$

The estimation for fk comes from the leaf weights, determined by minimizing the target function for the k_{th} tree, as shown in the equation below:

$$obj = \gamma T + \sum_{j=1}^{T} \left[G_j \omega_j + \frac{1}{2}(H_j + \lambda)\omega_j^2 \right] \tag{4}$$

In this setting, T represents the number of leaves in the k_{th} tree, with ω_j (where j ranges from 1 to T) signifying the weight attributed to each leaf. The parameters λ and γ are used to regulate the tree's structure and prevent overfitting. G_j and H_j denote the aggregated first and second gradients of the loss function, respectively, for all samples linked to the j_{th} leaf.

Building the k_{th} tree begins with a single leaf and involves an iterative process of splitting. This approach is guided by maximizing the gain parameter, as detailed below:

$$gain = \frac{1}{2}\left[\frac{G_L^2}{H_L + \lambda} + \frac{G_R^2}{H_R + \lambda} - \frac{(G_L + G_R)^2}{H_L + H_R + \lambda} \right] - \gamma \tag{5}$$

The formula presented above calculates the gain parameter, which is obtained from the G_L, H_L, G_R, and H_R values associated with the left and right leaves following a split. A split is deemed acceptable when the gain parameter exceeds 0. Raising the regularization parameters λ and γ reduces the gain parameter, promoting a less complex tree structure by restricting leaf splitting. Nevertheless, it's crucial to keep in mind that increasing these regularization parameters can decrease the model's capacity to fit the training data accurately.

3.2. Development of the XGBoost model

In this research, the XGBoost model was developed with Python and the Sklearn library. The focus was primarily on four key parameters: the learning rate (g), the number of estimators (N), and the regularization parameters (λ and γ). By concentrating on these four, the other parameters were left at their default settings in the XGBoost package, as they were deemed to have minimal impact on the model's performance. The training subset was then used to train the model.

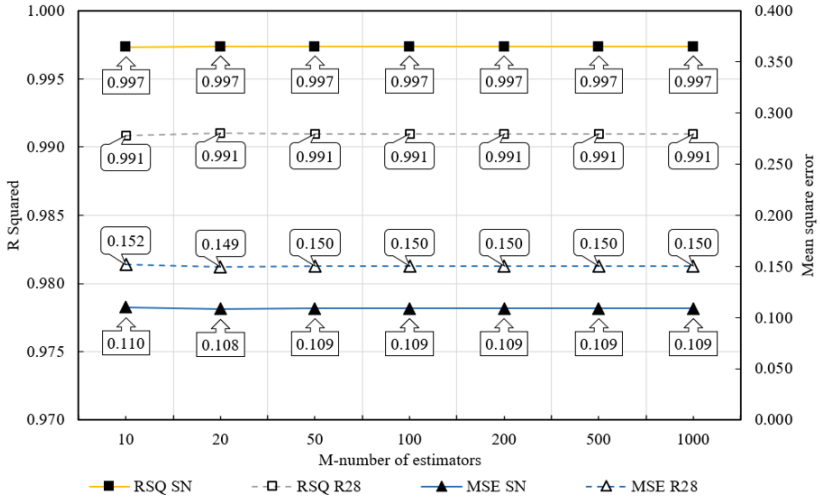

Figure 3. Impact of the number of estimators on model performance

The XGBoost model was trained using a wide range of estimator values, designated as N, ranging from 10 to 1000. The other parameters were kept at their default settings within the XGBoost package. Fig. 3 shows that the optimal RSQ and MSE values were achieved with 20 estimators. However, testing with 50 to 1000 estimators did not lead to any significant improvements over the performance seen with 20 estimators. Therefore, setting the estimator count to 20 proved to be the optimal decision, offering a balanced approach between precision and simplicity in the model.

The XGBoost model was trained over a spectrum of learning rates, ranging from 0.1 to 2, with the number of estimators fixed at the optimal value of 20. The other parameters were kept at their default settings. Fig. 4 indicates that the best RSQ and MSE results were obtained with a learning rate of 1.

To assess how sensitive the XGBoost model is to the regularization parameter λ, the number of estimators and learning rate were kept at their optimal settings: $N = 20$ and $\eta = 1$, as illustrated in Fig. 5. The parameter λ was tested over a range from 0.1 to 100. The results suggest that setting λ to 0 produces better results compared to other values in the given range.

Similarly, as demonstrated in Fig. 6, the impact of varying the regularization parameter γ on the XGBoost model was examined. Within the range from 0 to 10, the influence of γ appeared to be relatively small, with the model exhibiting slightly better performance when γ was set to 0.

According to the results, the ideal setup for the XGBoost model involved 20 estimators, a learning rate of 1, and regularization parameters λ and γ both set at 0. This configuration achieved the highest accuracy and will be employed for additional testing and validation. The time required to manually select the optimal parameters for the model is relatively long. However, the training time for the model is relatively short, taking less than 5 seconds.

Given the limited size of the experimental dataset, this study explores the effectiveness of applying the k-fold technique to enhance model generalization and mitigate overfitting. Fig. 7 illustrates the

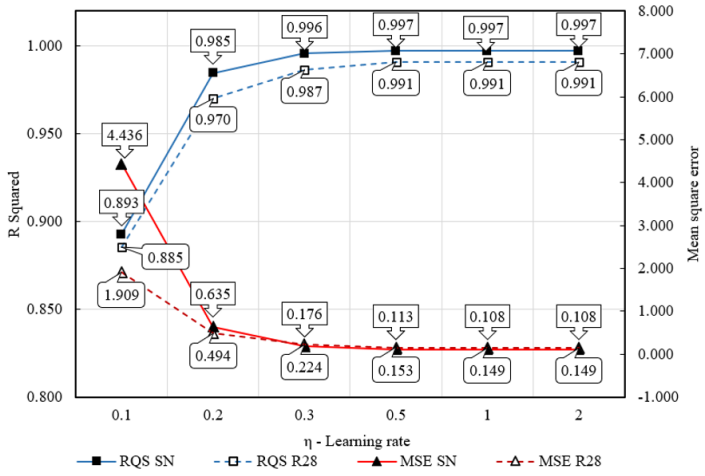

Figure 4. Impact of the learning rate on model performance

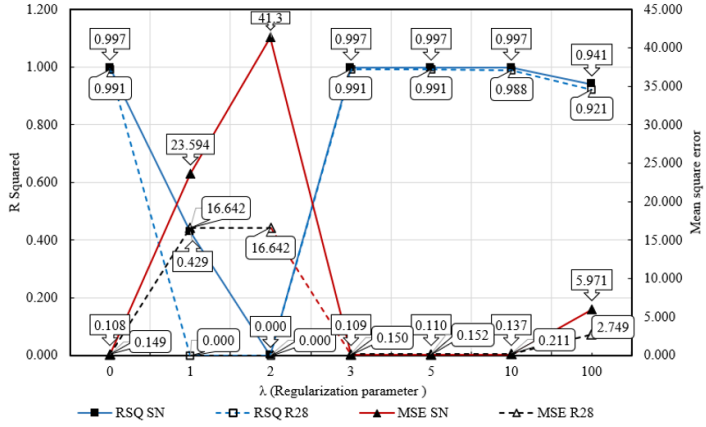

Figure 5. Impact of the regularization parameter λ on model performance

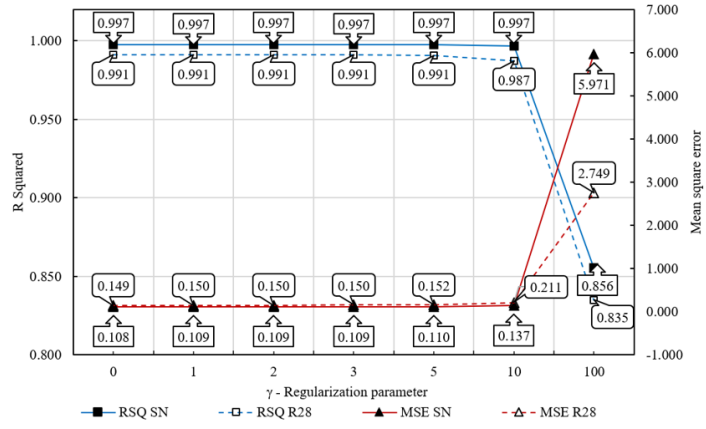

Figure 6. Impact of the regularization parameter γ on model performance

variation in R-squared and MSE values across different k-fold values. The results indicate that when k-fold is set to 3, the model achieves the highest accuracy for both slump and strength predictions of concrete.

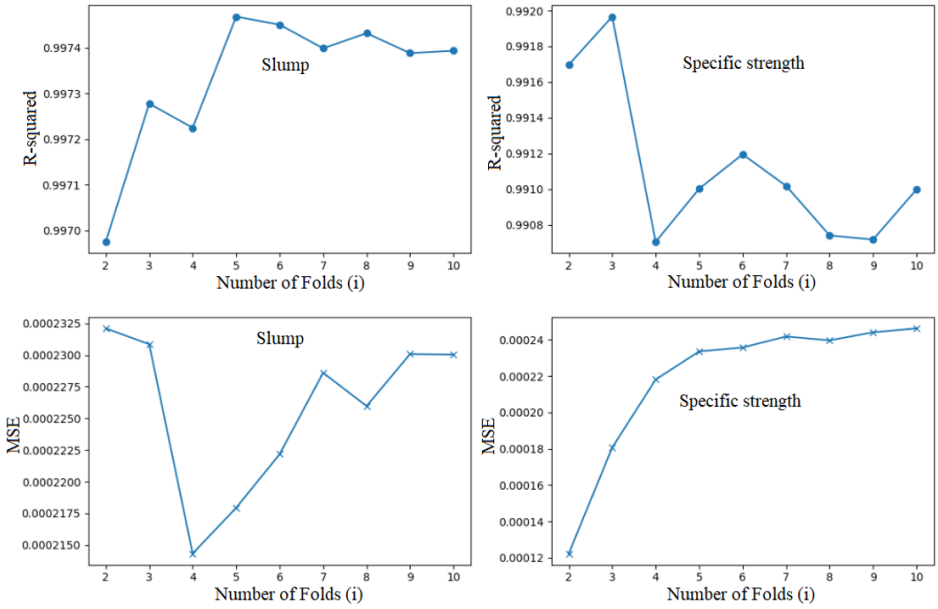

Figure 7. R-squared and MSE values across different k-fold values

4. Model validation

Figs. 8 and 9 depict the XGBoost model's performance on the training and validation datasets. The data indicates only minor deviations from the best fit line, suggesting a close correlation between the observed and expected outcomes. The evaluation metrics also demonstrate high precision in the training data, with R-squared scores of 0.997 for slump and 0.991 for specific strength, while the mean squared error (MSE) is 0.108 for slump and 0.149 for specific strength. These values are superior to those of a Random Forest (RF) model presented in [33]. Furthermore, applying the k-fold technique has improved the XGBoost model's accuracy and generalization, resulting in R-squared scores of 0.997 for slump and 0.992 for specific strength. The MSE values are also significantly lower, at 0.00023 for slump and 0.00018 for specific strength.

The XGBoost prediction model generates accurate results for the experimental dataset following the Box Hunter statistical method. The model occasionally predicts values that stray beyond the 5% deviation line, as shown in Figs. 7, 8, and Table 9 especially when handling data points that lie outside the training dataset's range. This result is consistent with the recognized constraints of empirical models; XGBoost typically performs more accurately with interpolation than with extrapolation. Additionally, if there are data points with identical output values but different input variables, it can lead to confusion in the XGBoost model, particularly when the training dataset is small (Fig. 7). Thus, enlarging the training dataset could enhance the XGBoost model's performance.

Additionally, the XGBoost model demonstrates higher accuracy in predicting strength parameters compared to slump parameters, as illustrated in Figs. 7, 8 and Table 9. Thus, prioritizing the construction of the XGBoost model to predict compressive strength is more efficient than utilizing it to forecast concrete slump.

Table 9 compares the predictive performance of the XGBoost model with and without the k-fold technique. While the k-fold model demonstrates higher accuracy on the training dataset, its predictive accuracy for concrete strength is lower than that of the model without k-fold. This discrepancy can be attributed to the small size of the test sample set and the potential for experimental errors.

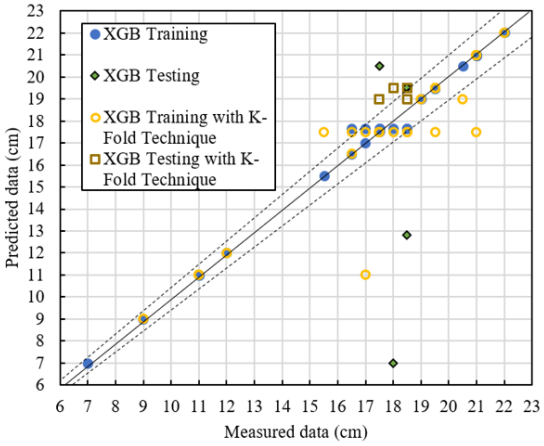

Figure 8. Scatterplots comparing predicted and measured data for slump

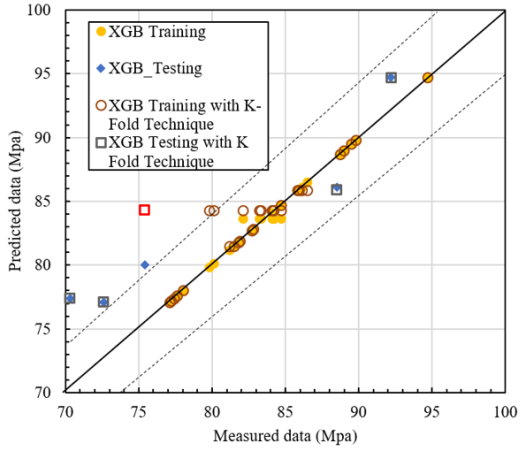

Figure 9. Scatterplots comparing predicted and measured data for specific strength

Table 9. Model accuracy (testing set)

No	Slump			Specific strength		
	Measured value (cm)	Predicted value (cm)	Predicted value with K-Fold (cm)	Measured value (Mpa)	Predicted value (Mpa)	Predicted value with K-Fold (Mpa)
1	18.5	12.83	19	92.2	94.70	94.7
2	17.5	20.50	19	88.5	86.10	85.90
3	18.5	19.50	19.5	75.4	79.99	84.30
4	18.5	19.50	19.5	72.6	77.10	77.1
5	18	7.00	19.5	70.3	77.40	77.40
Rsquared		0.0004	0.1667		0.9109	0.828
MSE		32.829	1.35		20.748	32.576

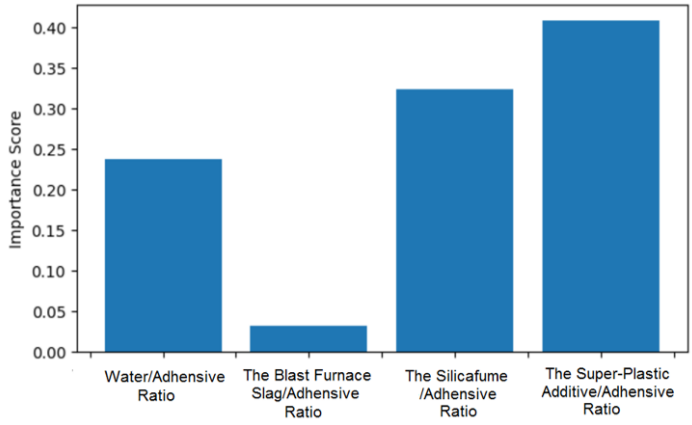

Figure 10. Features importance analysis

The feature importance analysis was conducted using the built-in functionality of the XGBoost algorithm, which evaluates feature significance based on gain, weight, or cover during training. The

results of this analysis are summarized in Fig. 10. As shown, the Super-Plastic Additive/Adhesive Ratio (x_4) emerged as the most influential factor in constructing the XGBoost model, with an importance score of 0.4078. The Silicafume/Adhesive Ratio (x_3) followed as the second most important variable, scoring 0.3241. These findings highlight the crucial role of the Super-Plastic Additive/Adhesive Ratio in determining the properties of concrete samples.

5. Conclusions

After producing concrete specimens with varying ratios of water/adhesive, blast furnace slag/adhesive, silica fume/adhesive, and super-plastic additive/adhesive to evaluate the optimal composition for high-performance concrete (HPC), along with developing an XGBoost prediction model to forecast the slump and compressive strength of these samples, the following conclusions can be drawn:

- Combining GGBFS and silica fume allows for creating concrete with exceptional properties, including a compressive strength exceeding 60 MPa and a slump measurement over 16 cm. This can be achieved while keeping the cement content under 300 kg/m^3 and limiting silica fume to less than 5%. Additionally, using GGBFS at 45%-55% of the total composition, along with adhesive and silica fume, does not hinder the early strength development rate compared to traditional concrete.

- The XGBoost model, developed using the experimental dataset following the Box-Hunter statistical method, is well-suited for predicting both the slump and compressive strength of concrete. However, it's important to note that the XGBoost model is more accurate in predicting compressive strength than slump. As a result, focusing on developing an XGBoost model for predicting concrete strength is considered more practical than constructing an XGBoost model for forecasting concrete slumps.

- While the XGBoost models generally achieved high accuracy in predicting concrete characteristics, and the k-fold technique improved generalizability, some predicted values still showed significant deviations from the observed measurements. This aligns with the fact that empirical models like XGBoost are best suited for interpolation tasks. To enhance the model's performance, it is crucial to expand the training dataset in both size and diversity to encompass a broader range of samples.

References

[1] Afshar, A., Jahandari, S., Rasekh, H., Shariati, M., Afshar, A., Shokrgozar, A. (2020). Corrosion resistance evaluation of rebars with various primers and coatings in concrete modified with different additives. *Construction and Building Materials*, 262:120034.

[2] Toghroli, A., Mehrabi, P., Shariati, M., Trung, N. T., Jahandari, S., Rasekh, H. (2020). Evaluating the use of recycled concrete aggregate and pozzolanic additives in fiber-reinforced pervious concrete with industrial and recycled fibers. *Construction and Building Materials*, 252:118997.

[3] Jahandari, S., Saberian, M., Tao, Z., Mojtahedi, S. F., Li, J., Ghasemi, M., Rezvani, S. S., Li, W. (2019). Effects of saturation degrees, freezing-thawing, and curing on geotechnical properties of lime and lime-cement concretes. *Cold Regions Science and Technology*, 160:242–251.

[4] Kazemi, M., Li, J., Lahouti Harehdasht, S., Yousefieh, N., Jahandari, S., Saberian, M. (2020). Non-linear behaviour of concrete beams reinforced with GFRP and CFRP bars grouted in sleeves. *Structures*, 23: 87–102.

[5] Sadeghian, F., Haddad, A., Jahandari, S., Rasekh, H., Ozbakkaloglu, T. (2021). Effects of electrokinetic phenomena on the load-bearing capacity of different steel and concrete piles: A small-scale experimental study. *Canadian Geotechnical Journal*, 58(5):741–746.

[6] Kazemi, M., Hajforoush, M., Talebi, P. K., Daneshfar, M., Shokrgozar, A., Jahandari, S., Saberian, M., Li, J. (2020). In-situ strength estimation of polypropylene fibre reinforced recycled aggregate concrete using Schmidt rebound hammer and point load test. *Journal of Sustainable Cement-Based Materials*, 9 (5):289–306.

[7] Rasekh, H., Joshaghani, A., Jahandari, S., Aslani, F., Ghodrat, M. (2020). Rheology and workability of SCC. In *Self-Compacting Concrete: Materials, Properties and Applications*, Elsevier, 31–63.

[8] Praveenkumar, S., Sankarasubramanian, G., Sindhu, S. (2019). Selecting optimized mix proportion of bagasse ash blended high performance concrete using analytical hierarchy process (AHP). *Computers and Concrete*, 23(6):459–470.

[9] Perumal, R. (2014). Performance and modeling of high-performance steel fiber reinforced concrete under impact loads. *Computers and Concrete*, 13(2):255–270.

[10] Ramadoss, P., Nagamani, K. (2013). Stress-strain behavior and toughness of high-performance steel fiber reinforced concrete in compression. *Computers and Concrete*, 11(2):149–167.

[11] Hoan, P. T., Thuong, N. T. (2019). Shear resistance of ultra-high-performance concrete reinforced with hybrid steel fiber subjected to impact loading. *Journal of Science and Technology in Civil Engineering (STCE) - NUCE*, 13(1):12–20.

[12] Hao, P. M., Thang, N. C., Thao, N. V., Tuan, N. V., Hai, L. N., Thuy, N. N., Man, N. X. (2022). Blast testing of ultra-high performance concrete fortifications using local materials. *Journal of Science and Technology in Civil Engineering (JSTCE) - HUCE*, 16(4):73–86.

[13] Tuan, N. V., Dong, P. S., Thanh, L. T., Thang, N. C., Hyeok, Y. K. (2021). Mix design of high-volume fly ash ultra high performance concrete. *Journal of Science and Technology in Civil Engineering (STCE) - HUCE*, 15(4):197–208.

[14] Mortazavi, S. N. S., Ince, A. (2020). An artificial neural network modeling approach for short and long fatigue crack propagation. *Computational Materials Science*, 185:109962.

[15] Castelli, M., Trujillo, L., Gonçalves, I., Popovič, A. (2017). An evolutionary system for the prediction of high performance concrete strength based on semantic genetic programming. *Computers and Concrete*, 19(6):651.

[16] Hung, T. V., Viet, V. Q., Thuat, D. V. (2019). A deep learning-based procedure for estimation of ultimate load carrying of steel trusses using advanced analysis. *Journal of Science and Technology in Civil Engineering (STCE) - NUCE*, 13(3):113–123.

[17] Li, S., Richard Liew, J. (2022). Experimental and Data-Driven analysis on compressive strength of steel fibre reinforced high strength concrete and mortar at elevated temperature. *Construction and Building Materials*, 341:127845.

[18] Duan, J., Asteris, P. G., Nguyen, H., Bui, X.-N., Moayedi, H. (2021). A novel artificial intelligence technique to predict compressive strength of recycled aggregate concrete using ICA-XGBoost model. *Engineering with Computers*, 37(4):3329–3346.

[19] Tipu, R. K., Panchal, V. R., Pandya, K. S. (2023). Multi-objective optimized high-strength concrete mix design using a hybrid machine learning and metaheuristic algorithm. *Asian Journal of Civil Engineering*, 24(3):849–867.

[20] Le, B.-A., Vu, V.-H., Seo, S.-Y., Tran, B.-V., Nguyen-Sy, T., Le, M.-C., Vu, T.-S. (2022). Predicting the compressive strength and the effective porosity of pervious concrete using machine learning methods. *KSCE Journal of Civil Engineering*, 26(11):4664–4679.

[21] Box, G. E. P., Hunter, W. H., Hunter, S. (1978). *Statistics for experimenters*, volume 664. John Wiley and Sons, New York.

[22] Kaïkea, A., Achoura, D., Duplan, F., Rizzuti, L. (2014). Effect of mineral admixtures and steel fiber volume contents on the behavior of high performance fiber reinforced concrete. *Materials & Design*, 63: 493–499.

[23] Melais, G. F. Z., Melais, S., Achoura, D., Jauberthie, R. (2015). Valorisation des sous-produits de hauts fourneaux dans la fabrication d'une nouvelle gamme de béton de sable (Valorisation of underproducts of blast furnaces in the manufacture of a new sandcrete range). *Journal of Materials and Environmental Science*, 6(3):735–742.

[24] Biskri, Y., Achoura, D., Chelghoum, N., Mouret, M. (2017). Mechanical and durability characteristics of High Performance Concrete containing steel slag and crystalized slag as aggregates. *Construction and Building Materials*, 150:167–178.

[25] Kourounis, S., Tsivilis, S., Tsakiridis, P., Papadimitriou, G., Tsibouki, Z. (2007). Properties and hydration

of blended cements with steelmaking slag. *Cement and Concrete Research*, 37(6):815–822.
[26] TCVN 6260:2020. *Blended portland cements*. Ministry of Science and Technology, Vietnam.
[27] TCVN 6016:2011. *Cement - Test methods - Determination of strength*. Ministry of Science and Technology, Vietnam.
[28] TCVN 6017:2015. *Cements - Test methods - Determination of setting time and soundness*. Ministry of Science and Technology, Vietnam.
[29] TCVN 13605:2023. *Cement – Test method for determination of fineness*. Ministry of Science and Technology, Vietnam.
[30] TCVN 7570:2006. *Aggregates for concrete and mortar–Specifications*. Ministry of Science and Technology, Vietnam.
[31] TCVN 7572:2006. *Aggregates for concrete and mortar - Test methods*. Ministry of Science and Technology, Vietnam.
[32] Chen, T., Guestrin, C. (2016). Xgboost: A scalable tree boosting system. In *Proceedings of the 22nd ACM SIGKDD International Conference on Knowledge Discovery and Data Mining*.
[33] Vu, V. T. (2023). Prediction of the slump and strength of high strength concrete using Random Forest model. *Journal of Science and Technique - Section on Special Construction Engineering*, 6(1):133–145.